

Theoretical and experimental study on intracavity pumped SrWO₄ anti-Stokes Raman laser

W. Wei · X. Y. Zhang · Q. P. Wang · C. Wang · Z. H. Cong ·
X. H. Chen · Z. J. Liu · W. T. Wang · Z. G. Wu · S. H. Ding ·
C. Y. Tu · Y. F. Li · W. Y. Cheng

Received: 15 September 2013 / Accepted: 20 November 2013 / Published online: 7 December 2013
© Springer-Verlag Berlin Heidelberg 2013

Abstract An intracavity pumped SrWO₄ anti-Stokes Raman laser is realized by placing an inclined SrWO₄ Raman cavity in a Q-switched Nd:YAG fundamental cavity. This structure is used to achieve non-collinear phase matching between the fundamental, the first-order Stokes and the first-order anti-Stokes waves. The maximum forward and backward first anti-Stokes outputs are 0.683 and 0.667 mJ, respectively, and the corresponding first anti-Stokes pulse widths are both 3.3 ns. A rate equation model is set up to simulate the output energies and temporal characteristics of these pulses. The stimulated results are in agreement with the experimental ones on the whole.

1 Introduction

Stimulated Raman scattering (SRS) is a significant method to obtain new laser wavelengths through nonlinear frequency conversion. With the emergence of excellent Raman crystals, solid-state Raman lasers have received much attention for the high Raman gain, compactness, good mechanical and thermal properties of these crystals [1–5]. Besides, Raman fiber laser sources with potential applications in optical communication [6] and medical optics [7, 8] also attract numerous concerns. Almost all these works have concentrated on the Stokes process. The frequency up-conversion in anti-Stokes process is a necessary supplement for the down-conversion in Stokes process. The generation of anti-Stokes waves can be an effective way to expand the spectral range of coherent light sources.

In most works, the anti-Stokes waves were generated by focusing ultrashort laser pulses into Raman crystals [9–12]. However, this focusing technique provides little control of the output spectrum and the output beam quality. An alternative approach is generating anti-Stokes waves in photonic crystal fibers, which has also attracted a lot of attention [13–15]. Nevertheless, the relatively low energy is not well suitable for most practical applications.

In 2004, A. A. Grasiuk et al. [16] realized effective first anti-Stokes generation at 511 nm using a two-stage Raman frequency converter. In the first stage, the first Stokes wave (wavelength 555 nm) was produced by pumping a potassium gadolinium tungstate (KGW) crystal with a small amount of the fundamental wave (wavelength 530 nm; pulse duration 20 ps). In the second stage, the first Stokes wave and the remaining fundamental wave were synchronously focused into another KGW crystal. On the condition of non-collinear phase matching between the fundamental,

W. Wei · X. Y. Zhang (✉) · Q. P. Wang · C. Wang ·
Z. H. Cong · X. H. Chen · Z. J. Liu · W. T. Wang · Z. G. Wu
School of Information Science and Engineering, Shandong
Provincial Key Laboratory of Laser Technology and
Application, Shandong University,
Jinan 250100, Shandong, China
e-mail: xyz@sdu.edu.cn

S. H. Ding
College of Photo-electronic Information Science and
Technology, Yantai University, Yantai 264005, Shandong,
China

C. Y. Tu
Fujian Institute of Research on the Structure of Matter, Chinese
Academy of Sciences, Fuzhou 350002, Fujian, China

Y. F. Li · W. Y. Cheng
Advanced Research Center for Optics, Shandong University,
Jinan 250100, Shandong, China

the first Stokes and the first anti-Stokes waves, the first anti-Stokes energy obtained was 8 μJ .

To achieve a more compact anti-Stokes laser source, in 2009, R. P. Mildren et al. [17] investigated a solid-state external cavity anti-Stokes Raman laser with a nanosecond pump laser and one KGW crystal. By parametric interaction between the fundamental (wavelength 532 nm; pulse duration 8 ns) and the generated first Stokes (wavelength 559 nm) beams, the maximum first anti-Stokes (wavelength 508 nm; pulse duration 4 ns) energy of 270 μJ was obtained.

The first anti-Stokes generation is a four-wave mixing (FWM) process [18], which depends on the intensities of both the fundamental wave and the SRS-generated first Stokes wave. In contrast to the extracavity pumped anti-Stokes Raman laser, intracavity pumped anti-Stokes systems have more advantages. The high intracavity fundamental wave intensity is propitious to the nonlinear conversion in the SRS and the FWM. And the intracavity anti-Stokes system uses round trips of the fundamental wave inside the Raman cavity. As far as we know, there are no relevant reports on either the theoretical model or the experimental research of the intracavity anti-Stokes Raman laser.

In this paper, an intracavity Q-switched Nd:YAG/SrWO₄ anti-Stokes laser is achieved. The spectral, the temporal and the phase-matching characteristics of the fundamental, the first Stokes and the first anti-Stokes outputs are studied. The maximum forward and backward first anti-Stokes energies are obtained to be 0.683 and 0.667 mJ, respectively, with the same pulse width 3.3 ns. In the theory part, we analyze the intracavity anti-Stokes laser based on rate equations, which are modified by adding additional terms to describe the conversion from the fundamental and the first Stokes waves to the first anti-Stokes wave. Numerically solving these equations, the temporal pulse shapes are simulated and the first anti-Stokes output energies are calculated. The stimulated results agree with the experimental ones on the whole.

2 Experimental setup

The experimental configuration of the intracavity Nd:YAG/SrWO₄ anti-Stokes laser is shown in Fig. 1. We arranged an inclined Raman cavity inside a Q-switched fundamental cavity to satisfy the phase matching of FWM. For the bidirectional output of the first anti-Stokes wave, two flash-lamp-pumped Nd:YAG rods (1.0 at.% doping concentration ϕ 5 mm \times 60 mm) were symmetrically placed on both sides of the Raman cavity. The rear mirror of the fundamental cavity (M_1) was high reflection (HR) coated at 1,064 nm ($R > 99.9\%$). The output coupler of the fundamental cavity (M_4) was high transmission (HT) coated for wavelengths 950–975 nm ($T > 99\%$) and partial reflection coated at 1,064 nm ($R = 83\%$). An aperture of 2 mm diameter was inserted near M_1 to maintain single-transverse-mode operation of the fundamental wave. The Raman medium was an a-cut SrWO₄ crystal with a size of 4 \times 4 \times 52 mm³. Both faces of the SrWO₄ crystal were anti-reflection (AR) coated at 1,064, 1,180 and 969 nm. The rear mirror of the Raman cavity (M_2) was coated for HR at 1,180 nm ($R > 99\%$). The output coupler of the Raman cavity (M_3) was coated for partial reflection at 1,180 nm ($R = 96\%$). The Raman cavity was located in a rotation stage (Zolix, RSA100) adjusted by a motion controller (Zolix, SC300-2B). The anti-Stokes laser operated at a pulse repetition rate of 1 Hz. The fundamental cavity length was 50 cm, and the Raman cavity length was 6.0 cm. All mirrors in this experiment were plane.

The output first anti-Stokes energies were measured by an energy sensor (Ophir, PE9-RoHS), connected to a laser energy meter (Ophir, NOVA II). The first anti-Stokes and the fundamental pulses were detected by a Si photodiode and the first Stokes pulses by an InGaAs photodiode. The pulse temporal behaviors were recorded with a digital phosphor oscilloscope (Tektronix, TDS3052B). The spectra of the laser waves were monitored and measured by an optical spectrum analyzer (Yokogawa, AQ6370C) of a spectral range from 600 to 1,700 nm.

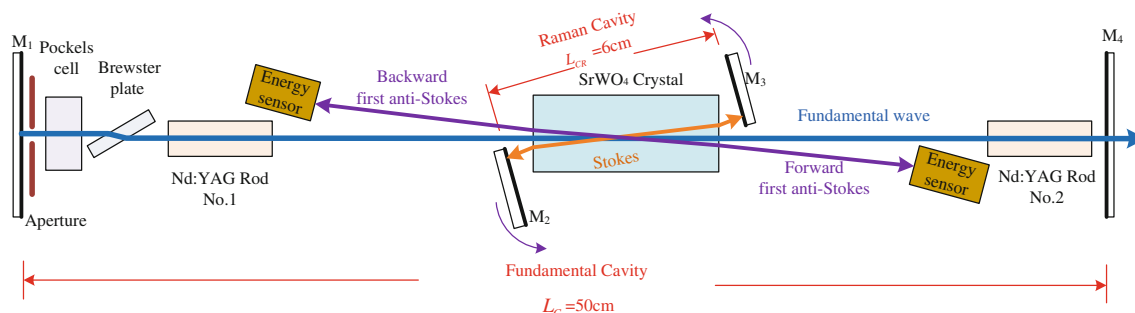


Fig. 1 Schematic diagram of the intracavity Nd:YAG/SrWO₄ anti-Stokes Raman laser

3 Experimental results and discussion

When the angle between the fundamental wave and the first Stokes wave (θ_{-1}) increased to approximately 0.93° , bidirectional first anti-Stokes beams emerged, and the maximum outputs were obtained with θ_{-1} rising up to about 1.90° . Corresponding to this, the optimal angle between the fundamental wave and the first anti-Stokes wave (θ_{+1}) was about 1.56° . These phase-matching angles are listed in Table 1.

The phase-matching angles were also calculated using the relation shown in Fig. 2. We compare them (also detailed in Table 1) with the experimental values. The

Table 1 The measured phase-matching angles compared with the calculated values

Output beam λ_i	Wavelength (nm)	Experimental angle θ_i ($^\circ$)	Calculated angle θ_i ($^\circ$)
First anti-Stokes λ_{+1}	969.1	$\theta_{+1} = 1.54 \pm 0.05$	$\theta_{+1} = 1.56$
Fundamental λ_0	1,064.2	$\theta_0 = 0.00 \pm 0.05$	$\theta_0 = 0$
First Stokes λ_{-1}	1,179.8	$\theta_{-1} = 1.92 \pm 0.15$	$\theta_{-1} = 1.90$

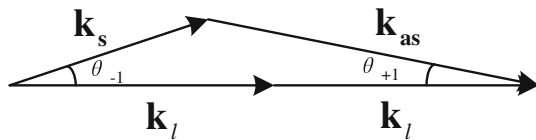
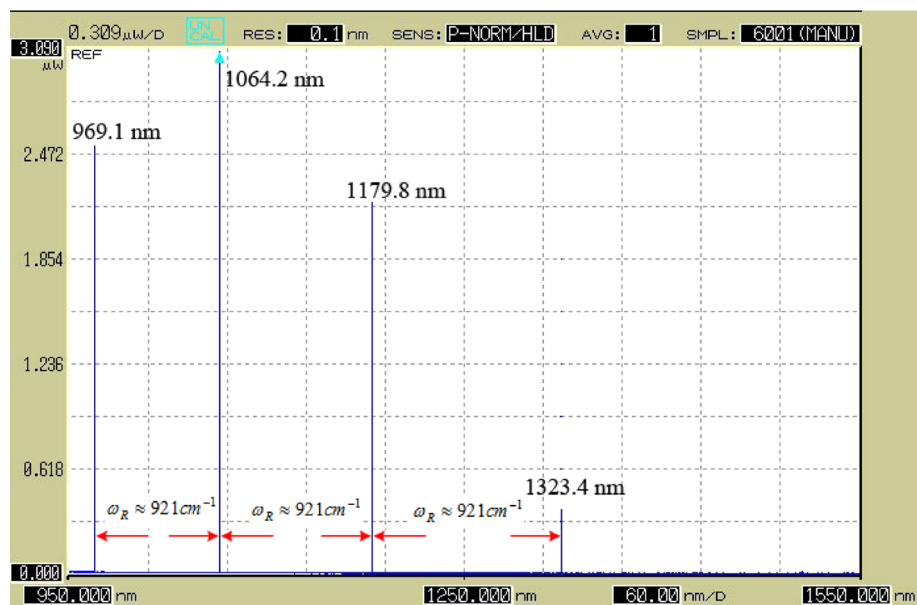


Fig. 2 Phase matching diagram for the first anti-Stokes generation. k_{as} , k_l and k_s are the first anti-Stokes, the fundamental and the first Stokes wave vectors, respectively

Fig. 3 The spectra of the first anti-Stokes, the fundamental, the first and the second Stokes outputs of the intracavity Nd:YAG/SrWO₄ anti-Stokes Raman laser



calculated angles are fairly consistent with the experimental ones. The minor differences are due to the deviation in the dispersion of the crystal from the published Sellmeier equations [19].

For the voltage applied on the flash lamp well above the threshold of Stokes generation, the first anti-Stokes, the fundamental, the first and the second Stokes outputs were observed at 969.1, 1,064.2, 1,179.8 and 1,323.4 nm as shown in the spectra of Fig. 3. The frequency shift between them agreed well with the optical vibration modes of tetrahedral WO_4^{2-} ionic groups of $SrWO_4$ (921 cm^{-1}) [20]. The first Stokes and the second Stokes waves were collinear, with the propagation direction defined by the Raman cavity. No apparent third Stokes wave around 1,506 nm was detected.

Figure 4 shows the forward and the backward output energies of the first anti-Stokes wave with respect to the pumping voltage. The forward first anti-Stokes energy shared the same variation trend with the backward counterpart and reached up to 0.683 mJ under the voltage of 775 V. The maximum backward one obtained was 0.667 mJ under the same pumping voltage.

The typical temporal behaviors of the laser pulses are shown in Fig. 5, in order to investigate the pulse temporal characteristics such as the pulse shapes, the pulse widths and the temporal correlation between pulses. The first anti-Stokes and the fundamental pulses are detected by the Si photodiode, and the first Stokes pulse is detected by the InGaAs photodiode. Therefore, the pulse profiles are not in scale with the respective pulse energies. The generation of the first Stokes wave occurred near the peak of the fundamental pulse. The first anti-Stokes pulse was just generated during the overlapping of the fundamental and the first

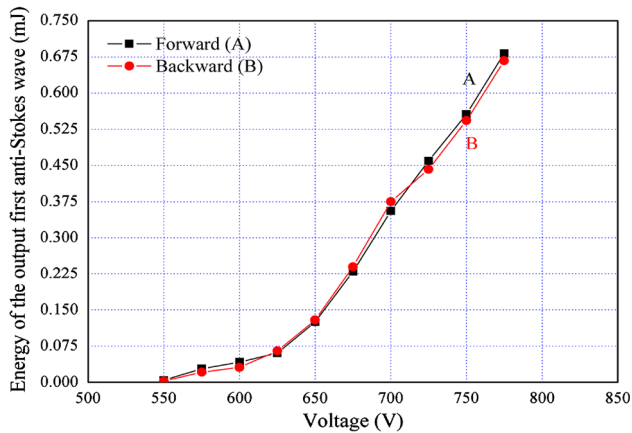


Fig. 4 Dependences of the bidirectional output first anti-Stokes energies on the pumping voltage. Curves correspond to different propagation directions as follows: *A* Forward. *B* Backward

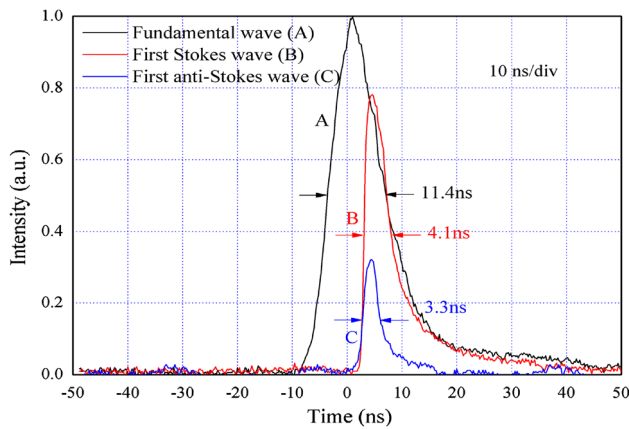


Fig. 5 Pulse profiles of the first anti-Stokes, the fundamental and the first Stokes waves

Stokes waves, which was in accordance with the FWM process. The pulse widths of the first anti-Stokes, the fundamental and the first Stokes waves were 3.3, 11.4 and 4.1 ns, respectively. No apparent difference was observed between the forward and backward temporal characteristics.

4 Theory

4.1 Rate equations for intracavity anti-Stokes lasers

In the intracavity anti-Stokes laser, the Raman cavity is placed inside the fundamental cavity. The first and the second Stokes waves oscillate in the Raman cavity, and the fundamental wave oscillate in the fundamental cavity.

In this paper, we assume the photon densities of the fundamental, the first anti-Stokes, the first Stokes and the second Stokes beams to be of plane-wave spatial distribution. And for flash-lamp-pumped lasers with gain media

like Nd:YAG, the initial population inversion density $n(0)$ can be considered to be uniform [21].

The walk-off angles between the fundamental and the Stokes waves are 1.04° and 1.90° inside and outside the SrWO₄ crystal, respectively. Considering the symmetry of the Raman cavity, the maximal departure between the fundamental and the first Stokes beams is <0.5 mm in the SrWO₄ crystal. The walk-off between the fundamental and the first anti-Stokes beams is smaller. Thus, it is reasonable to regard the first anti-stokes, the fundamental, the first and the second Stokes waves as collinear.

By taking the conversion from the fundamental and the first Stokes waves to the first anti-Stokes wave into account and considering the variation of the second Stokes photon density, the rate equations of actively Q-switched intracavity Raman lasers in Ref. [22] are modified as

$$\frac{d\phi_1(t)}{dt} = \frac{2\sigma n(t)\phi_1(t)L}{t_r} - \frac{2g\hbar\omega_s c\phi_r(t)\phi_s(t)L_R}{t_r/[L_{a-1} - \ln(R_1)]} - \left. \frac{d\phi_1(t)}{dt} \right|_{\text{FWM}}, \quad (1a)$$

$$\frac{d\phi_s(t)}{dt} = \frac{2g_1\hbar\omega_s c\phi_r(t)\phi_s(t)L_R}{t_{rs}/[L_{a-s} - \ln(R_s)]} - \frac{\phi_s(t)}{t_{rs}} + K_{sp}\phi_r(t) + \left. \frac{d\phi_s(t)}{dt} \right|_{\text{FWM}}, \quad (1b)$$

$$\frac{dn(t)}{dt} = -\gamma c\sigma n(t)\phi_1(t) - \frac{n(t)}{\tau_g}, \quad (1c)$$

$$\frac{d\phi_{s2}(t)}{dt} = \frac{2g_2\hbar\omega_{s2} c\phi_s(t)\phi_{s2}(t)L_R}{t_{rs}} - \frac{\phi_{s2}(t)}{t_{rs}/[L_{a-s2} - \ln(R_{s2})]} + K_{sp2}\phi_s(t), \quad (1d)$$

where $\phi_1(t)$ and $\phi_r(t)$ are the fundamental photon densities in the gain medium and in the Raman medium, respectively. Because of the continuity of energy flux inside the resonator, the fundamental photon densities satisfy the relation $W_1^2\phi_1(t) = W_r^2\phi_r(t)$, where W_1 and W_r are the beam radii of the fundamental wave in the gain medium and in the Raman medium. $\phi_s(t)$ and $\phi_{s2}(t)$ are the first and the second Stokes photon densities in the Raman medium; $n(t)$ is the population inversion density. ω_1 , ω_s and ω_{s2} are the fundamental, the first and the second Stokes angular frequencies, respectively; g is the Raman gain coefficient for the fundamental wave; $g_1 = (\omega_s/\omega_1)g$ and $g_2 = (\omega_{s2}/\omega_1)g$ are the Raman gain coefficients for the first and the second Stokes waves; K_{sp} and K_{sp2} are the spontaneous Raman scattering factors of the first and the second Stokes. h is the Planck constant with $\hbar = h/(2\pi)$; c is the light speed in vacuum; L and L_R are the lengths of the gain medium and the Raman crystal, respectively; γ is the

inversion reduction factor of the gain medium; σ is the stimulated emission cross section of the gain medium; τ_g is the fluorescence lifetime of the upper level in the gain medium. t_r is the round-trip transit time of the fundamental wave, and t_{rs} is the round-trip transit time of the first and the second Stokes waves, ignoring the small optical path difference between them. L_{a-1} , L_{a-s} and L_{a-s2} are the intrinsic losses of the fundamental, the first Stokes and the second Stokes waves; R_1 is the reflectivity of the fundamental output coupler (M_4 in Fig. 1) at the fundamental wavelength; R_s and R_{s2} are the reflectivities of the Raman output coupler (M_3 in Fig. 1) at the first and the second Stokes wavelengths. $d\phi_1(t)/dt|_{\text{FWM}}$ is the loss rate of the fundamental photon density caused by the FWM. $d\phi_s(t)/dt|_{\text{FWM}}$ is the generation rate of the first Stokes photon density caused by the same process.

4.2 First anti-Stokes intensity and single-pulse energy

In the slowly varying amplitude approximation, the spatial evolution of the forward first anti-Stokes field amplitude E_{as} is given by [23]

$$\frac{dE_{as}}{dz} = \frac{i\omega_{as}}{2n_{as}c\epsilon_0} \mathbf{P}^{(3)}(\omega_{as}) e^{-ik_{as}z}, \tag{2}$$

where the polarization coefficient is defined through the expression

$$\mathbf{P}^{(3)}(\omega_{as}) = 6\epsilon_0\chi_R^{(3)}(\omega_{as}; \omega_1, -\omega_1, \omega_{as}) |E_1|^2 E_{as} e^{ik_{as}z} + 3\epsilon_0\chi_F^{(3)}(\omega_{as}; \omega_1, \omega_1, -\omega_s) E_1^2 E_s^* e^{i(2k_1 - k_s)z}, \tag{3}$$

where the first item of $\mathbf{P}^{(3)}(\omega_{as})$ represents the loss of the first anti-Stokes wave caused by its conversion to the fundamental wave, and the second item represents the first anti-Stokes generation caused by the FWM. k_{as} , k_1 and k_s are the first anti-Stokes, the fundamental and the first Stokes wave vectors, respectively; E_1 and E_s are the fundamental and the first Stokes field amplitudes; n_{as} is the refractive index of the first anti-Stokes wave; ω_{as} is the first anti-Stokes angular frequency; ϵ_0 is the permittivity of free space. $\chi_R^{(3)}(\omega_{as})$ is the anti-Stokes Raman susceptibility, and $\chi_F^{(3)}(\omega_{as})$ is the anti-Stokes FWM susceptibility. $\chi_F^{(3)}(\omega_{as})$ is related to $\chi_R^{(3)}(\omega_{as})$ by [23]

$$\chi_F^{(3)}(\omega_{as}) = 2\chi_R^{(3)}(\omega_{as}). \tag{4a}$$

$\chi_R^{(3)}(\omega_{as})$ is related to the Stokes Raman susceptibility $\chi_R^{(3)}(\omega_s)$ through [24]

$$\chi_R^{(3)}(\omega_{as}) = \chi_R^{(3)}(\omega_s)^*. \tag{4b}$$

Here, $\chi_R^{(3)}(\omega_s)$ is separated into the real part and the imaginary part as

$$\chi_R^{(3)}(\omega_s) = \chi_R'(\omega_s) + i\chi_R''(\omega_s). \tag{4c}$$

Near the Raman resonance, the real part $\chi_R'(\omega_s)$ can be approximated to be 0 [23], and the imaginary part $\chi_R''(\omega_s)$ can be calculated through [18]

$$g = -\frac{8\pi\omega_s}{\epsilon_0 c^2 n_1 n_s} \chi_R''(\omega_s), \tag{5}$$

where n_s and n_1 are the refractive indexes of the first Stokes wave and the fundamental wave.

Because $|E_{as}|$ is much lower than $|E_s|$, the first item of Eq. (3) can be neglected compared with the second one, and the variation of the fundamental and the first Stokes waves for the generation of the first anti-Stokes wave is negligible too. Therefore, Eq. (2) is rewritten as

$$\frac{dE_{as}}{dz} = \frac{i3\omega_{as}}{2n_{as}c} \chi_F^{(3)}(\omega_{as}) E_1^2 E_s^* e^{i(2k_1 - k_s)z}. \tag{6}$$

The forward first anti-Stokes energy equals to 0 at the back end of the SrWO₄ crystal and increases to the maximum value at the front end. On the contrary, the backward one equals to 0 at the front end of the crystal and rises up to the highest at the back end.

$$E_{as\text{-forward}}(z)|_{z=0} = 0, \quad E_{as\text{-forward}}(z)|_{z=L_R} = \max(E_{as\text{-forward}}), \tag{7a}$$

$$E_{as\text{-backward}}(z)|_{z=L_R} = 0, \quad E_{as\text{-backward}}(z)|_{z=0} = \max(E_{as\text{-backward}}). \tag{7b}$$

Considering the symmetry of the intracavity FWM, the bidirectional first anti-Stokes energies can be regarded as the same.

Integrating Eq. (6) from 0 to the length of the Raman crystal L_R with

$$I_i = \frac{1}{2} \epsilon_0 c n_i |E_i|^2 \quad (i = l, s, as), \tag{8}$$

and using the relations (4a–4c) and (5), the one-way output first anti-Stokes intensity $I_{as}(t)$ is given by

$$I_{as}(t) = \frac{9n_s\omega_{as}^2 g^2 L_R^2}{16\pi^2 n_{as}\omega_s^2} \text{sinc}^2\left(\frac{\Delta k L_R}{2}\right) \left[\frac{1}{2} I_1(t)\right]^2 \cdot \left[\frac{1}{2} I_s(t)\right], \tag{9}$$

where Δk is the wave vector mismatch given by

$$\Delta k = 2k_1 - k_{as} - k_s. \tag{10}$$

On the condition of phase matching (i.e., $\Delta k = 0$ in Eq. (10)), Eq. (9) is rewritten as

$$I_{as}(t) = \frac{9n_s\omega_{as}^2 g^2 L_R^2}{128\pi^2 n_{as}\omega_s^2} I_1^2(t) I_s(t). \tag{11}$$

By using the relation between photon densities and optical intensities of the fundamental and the first Stokes

waves, $I_i(t) = \phi_i(t)c\hbar\omega_i$, ($i = 1, s$), the one-way output intensity $I_{as}(t)$ and the single-pulse energy E_{as} of the first anti-Stokes wave can be expressed as

$$I_{as}(t) = \frac{9c^3\hbar^3 n_s \omega_1^2 \omega_{as}^2 g^2 L_R^2}{128\pi^2 n_{as} \omega_s} \phi_1^2(t) \phi_s(t), \tag{12}$$

$$E_{as} = \int_0^\infty I_{as}(t) A_{as} dt \tag{13}$$

$$= \frac{9c^3\hbar^3 n_s \omega_1^2 \omega_{as}^2 g^2 L_R^2 A_{as}}{128\pi^2 n_{as} \omega_s} \int_0^\infty \phi_1^2(t) \phi_s(t) dt$$

where A_{as} is the area of the first anti-Stokes beam.

The fundamental, the first Stokes and the second Stokes output energies E_1 , E_s and E_{s2} can be expressed as

$$E_1 = \frac{1}{2} \ln\left(\frac{1}{R_1}\right) c\hbar\omega_1 A_1 \int_0^\infty \phi_1(t) dt, \tag{14a}$$

$$E_s = \frac{1}{2} \ln\left(\frac{1}{R_s}\right) c\hbar\omega_s A_s \int_0^\infty \phi_s(t) dt, \tag{14b}$$

$$E_{s2} = \frac{1}{2} \ln\left(\frac{1}{R_{s2}}\right) c\hbar\omega_{s2} A_{s2} \int_0^\infty \phi_{s2}(t) dt, \tag{14c}$$

where A_1 , A_s and A_{s2} are the beam areas of the fundamental, the first Stokes and the second Stokes waves, respectively.

According to the photon number conservation and the photon energy conservation in the FWM process, a first anti-Stokes photon is generated along with the consumption of two fundamental photons and the generation of a first Stokes photon. Thus, the variation rates of the fundamental and the first Stokes photon densities satisfy the following relation:

$$\frac{1}{2} \times \frac{L_C}{L_{CR}} \frac{d\phi_l}{dt} \Big|_{FWM} = \frac{d\phi_s}{dt} \Big|_{FWM} = \frac{2I_{as}(t)}{\hbar\omega_{as}L_{CR}}, \tag{15}$$

where L_C and L_{CR} are the optical lengths of the fundamental cavity and the Raman cavity, respectively. $2I_{as}(t)$ is the total first anti-Stokes intensity in consideration of the consistency of the forward and the backward anti-Stokes waves.

Substituting Eq. (12) into Eq. (15) and substituting the obtained variation rates into Eqs. (1a–1d), the rate equations can be numerically solved. Substituting $\phi_1(t)$ and $\phi_s(t)$ into Eqs. (12) and (13), we can calculate the one-way output intensity and the pulse energy of the first anti-Stokes wave.

4.3 Numerical calculation

We give the theoretical simulation results of the temporal shapes and the one-way output first anti-Stokes energy for

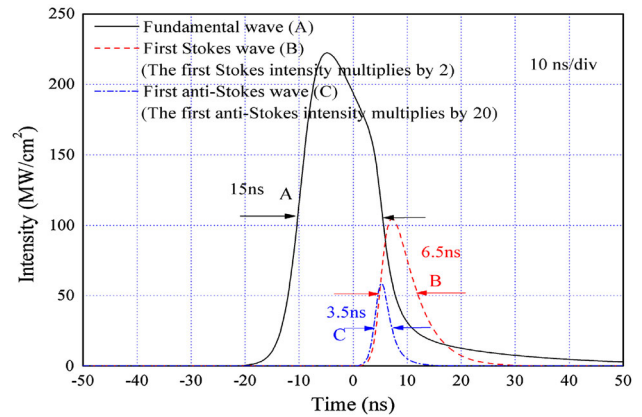


Fig. 6 Simulated pulse profiles of the fundamental, the first Stokes and the first anti-Stokes waves with pulse durations about 15, 6.5 and 3.5 ns, respectively

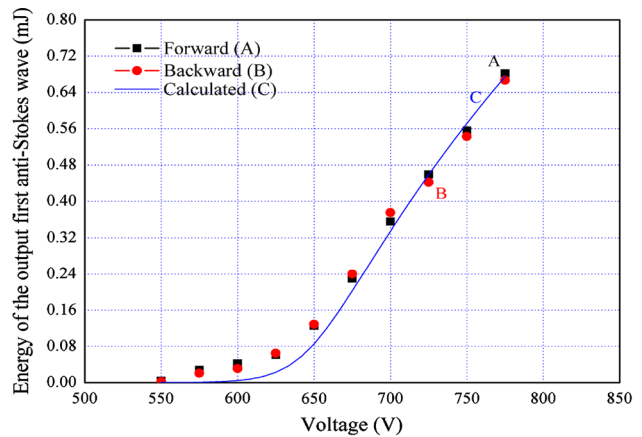


Fig. 7 Theoretical and experimental output first anti-Stokes energies with respect to the pumping voltage. The symbols *A* and *B* are the experimental results, and the curve *C* is the theoretical result

comparison. The shapes were simulated at the pumping voltage of 775 V as shown in Fig. 6. For showing the pulse temporal characteristics clearly, the intensity of the first Stokes wave was multiplied by 2, and the intensity of the first anti-Stokes wave was multiplied by 20. The pulse durations of the fundamental, the first Stokes and the first anti-Stokes waves are about 15, 6.5 and 3.5 ns, respectively. The one-way output energy with respect to the pumping voltage was calculated from 500 to 850 V as shown in Fig. 7 (Curve C). The parameters for the numerical calculation are listed in Table 2.

We can see that the theoretical temporal characteristics in Fig. 6 are in accordance with the experimental results shown in Fig. 5 on the whole. The calculated one-way output first anti-Stokes energy versus the pumping voltage shares the same variation trend with the experimental results. Some discrepancies can also be observed, and the reasons may be as follows: Firstly, our theoretical model was obtained under the collinear approximation. In the

Table 2 Parameters for simulations

Parameters	Values	Ref.
σ	Stimulated emission cross section of Nd:YAG crystals	$6.5 \times 10^{-19} \text{ cm}^2$ [25]
γ	Inversion reduction factor of Nd:YAG crystals	0.60
τ_g	Fluorescence lifetime of the upper level in Nd:YAG crystals	230 μs [25]
g	Raman gain coefficient	5.0 cm/GW [20]
L	Length of the Nd:YAG crystal	60 mm
L_c	Length of the fundamental cavity	50 cm
L_R	Length of the SrWO ₄ crystal	52 mm
L_{CR}	Length of the Raman cavity	6.0 cm
n	Refractive index of the fundamental wave in Nd:YAG	1.82 [25]
n_{as}	Refractive index of the first anti-Stokes wave in SrWO ₄	1.8363 [19]
n_1	Refractive index of the fundamental wave in SrWO ₄	1.8322 [19]
n_s	Refractive index of the first Stokes wave in SrWO ₄	1.8278 [19]
n_{s2}	Refractive index of the second Stokes wave in SrWO ₄	1.8228 [19]
K_{sp}	Spontaneous first Stokes scattering factor	2×10^{-6}
K_{sp2}	Spontaneous second Stokes scattering factor	2×10^{-6}
R_1	Reflectivity of the fundamental output coupler at 1,064 nm	83 %
R_s	Reflectivity of the Raman cavity output couple at 1,180 nm	96 %
R_{s2}	Reflectivity of the Raman cavity output couple at 1,323 nm	30 %
W_{as}	Radius of the first anti-Stokes beam	1.5 mm
ω_R	SRS frequency shift of SrWO ₄ crystals	921 cm^{-1}

experiment, the fundamental, the first Stokes and the first anti-Stokes waves satisfied the non-collinear phase matching. The walk-off angles for the non-collinear phase matching can impact the spatial overlapping of the laser beams. Secondly, we assumed the laser beams to be of plane-wave spatial distribution. That is to say, the photon densities only depended on time in the rate equation model. In fact, they also depended on space. Thirdly, the intrinsic losses L_{a-1} , L_{a-s} and L_{a-s2} used in the calculation were not very accurate. Different values of L_{a-1} , L_{a-s} and L_{a-s2} also influenced the calculated pulse shapes.

5 Conclusions

In summary, an intracavity Nd:YAG/SrWO₄ anti-Stokes Raman laser has been studied theoretically and

experimentally. The phase-matching conditions, the spectrum and the temporal characteristics of the fundamental, the first Stokes and the first anti-Stokes waves are investigated. The maximum forward and backward output energies of the first anti-Stokes wave were 0.683 and 0.667 mJ, respectively. In addition, we derived the expressions of the first anti-Stokes energy and optical intensity and modified the rate equation model for intracavity anti-Stokes Raman lasers. This model was used to analyze the performance of this Nd:YAG/SrWO₄ anti-Stokes laser. The simulated results were consistent with the experimental ones on the whole. This model can also be used to predict the characteristics of other intracavity pumped anti-Stokes Raman lasers.

Acknowledgments This research is supported by the National Natural Science Foundation of China (11174185, 10974168), the Research Fund for the Doctoral Program of Higher Education of China (20100131110064).

References

1. H.M. Pask, Prog. Quantum Electron. **27**, 3 (2003)
2. P. Cerny, H. Jelinkova, P.G. Zverev, T.T. Basiev, Prog. Quantum Electron. **28**, 113 (2004)
3. Y.F. Chen, Opt. Lett. **29**, 2172 (2004)
4. A.J. Lee, H.M. Pask, P. Dekker, J.A. Piper, Opt. Lett. **35**, 682 (2010)
5. J.P.M. Feve, K.E. Shortoff, M.J. Bohn, J.K. Bresseur, Opt. Express **19**, 913 (2011)
6. N.S. Kim, M. Prabhu, C. Li, J. Song, K. Ueda, Opt. Commun. **176**, 219 (2000)
7. J.F. Andersen, J. Busck, H. Heiselberg, Appl. Opt. **45**, 6198–6204 (2006)
8. P. Hajireza, A. Forbrich, Y. Jiang, W. Shi, R. Zemp, Proc. SPIE **8581**, 858129–858131 (2013)
9. A.A. Kaminskii, H.J. Eichler, K. Ueda, N.V. Klassen, B.S. Redkin, L.E. Li, J. Findeisen, D. Jaque, J. García-Sole, J. Fernández, R. Balda, Appl. Opt. **21**, 4533 (1999)
10. A.A. Kaminskii, S.N. Bagaev, K. Ueda, K. Takaichi, H.J. Eichler, Crystallogr. Rep. **47**, 653 (2002)
11. D.W. Hu, Z.P. Wang, H.J. Zhang, X.G. Xu, J.Y. Wang, Z.S. Shao, Chin. Phys. Lett. **23**, 2766 (2006)
12. A.A. Kaminskii, H. Rhee, H.J. Eichler, L. Bohaty, P. Becker, K. Takaichi, Laser Phys. Lett. **5**, 304 (2008)
13. E.R. Andresen, S.R. Keiding, E.O. Potma, Opt. Express **14**, 7246 (2006)
14. S.O. Konorov, E.E. Serebryannikov, A.M. Zheltikov, P. Zhou, A.P. Tarasevitch, D. von der Linde, Opt. Lett. **29**, 1545 (2004)
15. F. Benabid, J.C. Knight, G. Antonopoulos, P. St. J. Russell Sci. **298**, 399 (2002)
16. A.Z. Grasiuk, S.V. Kurbasov, L.L. Losev, Opt. Commun. **240**, 239 (2004)
17. R.P. Mildren, D.W. Coutts, D.J. Spence, Opt. Express **17**, 810 (2009)
18. Y.R. Shen, *The principles of nonlinear optics* (Wiley, New York, 1984)
19. A.M. Prokhorov, Yu. S. Kuz'minov, *Ferroelectric crystals for laser radiation control* (Adam Hilger, Bristol, 1990)
20. S.H. Ding, X.Z. Zhang, Q.P. Wang, F.F. Su, S.T. Li, S.Z. Fan, Z.J. Liu, J. Chang, S.S. Zhang, S.M. Wang, Y.R. Liu, IEEE J. Quantum Electron. **42**, 78 (2006)

21. X.Y. Zhang, S.Z. Zhao, Q.P. Wang, *J. Opt. Soc. Am. B* **17**, 1166 (2000)
22. S.H. Ding, X.Y. Zhang, Q.P. Wang, J. Chang, S.M. Wang, Y.R. Liu, *IEEE J. Quantum Electron.* **43**, 722 (2007)
23. R.W. Boyd, *Nonlinear optics* (Elsevier Pte Ltd, Singapore, 2010)
24. N. Bloembergen, *Nonlinear optics* (W. A. Benjamin, New York, 1965)
25. H. Hemmati, *OSA Proc. Adv. Solid State Lasers* **10**, 257 (1991)